# Soft Matter



**View Article Online PAPER** 



Cite this: Soft Matter, 2024, 20.1459

Received 3rd October 2023, Accepted 10th January 2024

DOI: 10.1039/d3sm01324c

rsc.li/soft-matter-journal

# Sliding friction of a pillar array interface: part II, contact mechanics of single pillar pairs†

Xuemei Xiao, ‡ Jasreen Kaur, ‡ Bangguo Zhu, Anand Jagota \*\* \*\* and 

Insects and small animals often utilize structured surfaces to create friction during their movements. These surfaces typically consist of pillar-like fibrils that interact with a counter surface. Understanding the mechanical interaction between such surfaces is crucial for designing structured surfaces for engineering applications. In the first part of our study, we examined friction between poly(dimethylsiloxane) (PDMS) samples with surfaces patterned with pillar-arrays. We observed that sliding between these surfaces occurs through the interfacial glide of dislocation structures. The frictional force that resists this dislocation glide is a result of periodic single pillar-pillar contact and sliding. Hence, comprehending the intricate interaction between individual pillar contacts is a fundamental prerequisite for accurately modeling the friction behavior of the pillar array. In this second part of the study, we thoroughly investigated the contact interaction between two pillars located on opposite sides of an interface, with different lateral and vertical offsets. We conducted experiments using PDMS pillars to measure both the reaction shear and normal forces. Contact interaction between pillars was then studied using finite element (FE) simulations with the Coulomb friction model, which yielded results that aligned well with the experimental data. Our result offers a fundamental solution for comprehending how fibrillar surfaces contact and interact during sliding, which has broad applications in both natural and artificial surfaces.

#### 1. Introduction

The ability to control friction between soft and hard surfaces through surface architecture has various engineering applications, such as automobile tires and locomotion of soft robots.<sup>1</sup> Over the last two decades, the design of textured surfaces has been influenced by the adhesive properties observed in small animals and insects, such as geckos rapidly climbing vertical walls.<sup>2</sup> This inspiration has led researchers to develop fibrillar surfaces to enhance and control adhesion and friction.<sup>3-11</sup> Typically, these surfaces consist of micro-pillars or fibrils arranged in arrays, allowing for flexible contact with hard surfaces.3-11 While many successful examples have utilized relatively soft elastomers, other materials like carbon nanotube arrays have been used to create compliant surfaces with

In Part I of this work, 18 we presented a study of the friction between poly(dimethylsiloxane) (PDMS) samples with surfaces patterned with pillar arrays. We demonstrated that the relative sliding motion is accommodated by the interfacial glide of surface dislocations. The mechanics of contact during sliding are highly complex, as the pillars are nonlinearly elastic and undergo significant rotation during bending. Additionally, the shape and size of the contact area during sliding are influenced by friction, local deformation, and global changes in geometry

significantly increased friction. 12,13 Polypropylene pillar arrays have demonstrated a dramatic increase in friction, 14 and soft pillar arrays with moderate to small aspect ratios have also shown enhanced friction. Shen et al.15 demonstrated that a film-terminated fibrillar interface can greatly enhance static friction. Varenberg et al.16 fabricated a low aspect ratio hexagonal micro-array made of polyvinyl siloxane (PVS) to control wet and dry friction. Kim et al.17 utilized an array of soft polyurethane pillars with spatulate tips, resulting in a significant increase in friction when sliding against a flat surface made of the same material. It is worth noting that in much of the aforementioned work, the pillar array was tested against an unstructured, flat, and occasionally rough surface. Furthermore, there is a lack of experimental studies or theoretical analysis on the contact interaction between individual pillars in the array.

<sup>&</sup>lt;sup>a</sup> Department of Mechanical and Aerospace Engineering, Cornell University, Ithaca, NY 14853, USA. E-mail: ch45@cornell.edu

<sup>&</sup>lt;sup>b</sup> Department of Chemical and Biomolecular Engineering, Lehigh University, Bethlehem, PA 18015, USA. E-mail: anj6@lehigh.edu

<sup>&</sup>lt;sup>c</sup> Department of Bioengineering, Lehigh University, Bethlehem, PA 18015, USA

<sup>&</sup>lt;sup>d</sup> Global Station for Soft Matter, GI-CoRE, Hokkaido University, Sapporo, Japan

<sup>†</sup> Electronic supplementary information (ESI) available. See DOI: https://doi.org/ 10.1039/d3sm01324c

<sup>‡</sup> These authors contributed equally.

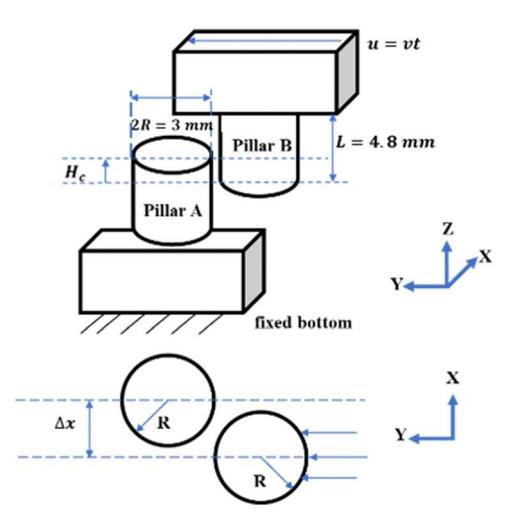


Fig. 1 Geometry of single pillar pair (SPP) sample. The substrate of the bottom sample is fixed and the upper PDMS substrate moves in the y direction with constant speed v. The height of contact is  $H_c$  and the lateral offset is  $\Lambda x$ .

caused by large rotations. In our experiments, the aspect ratio of the soft pillars (height/radius) is 3.2, making the conventional beam bending theory inadequate for accurately describing global deformation. Moreover, there are other complications arising from misalignments between pillars in the array, which are caused by misorientation and vertical separation. For the single pillar pair (SPP), the misorientation and vertical separations are represented by lateral and vertical offsets, as illustrated in Fig. 1.

In Part II of this work, we present an experimental and modeling study on the mechanics of two elastomeric pillars in sliding contact. Our experiments are designed to measure the sliding force between two pillars as they come into contact and eventually separate when the contact becomes unstable. We control the vertical separation (or height of contact) and the horizontal separation (or lateral offset) in our sliding experiments (refer to Fig. 1 and the section on geometry). The results from a 3D Finite Element (FE) simulation, using a Coulomb friction model for interfacial tractions on the contacting surfaces, are fitted to the experimental data.

The plan of this paper is as follows. In Section 2 we give details about the specimen geometry, the experimental method and material selection. Details of the FE simulations are given in Section 3. Comparison of FE and experimental results are in Section 4. We conclude in Section 5 with a summary and discussion.

## 2. Geometry

Fig. 1 shows the specimen geometry. The SPP samples consist of two identical PDMS pillars on two identical PDMS substrates (see 2.1 for fabrication process). Each pillar is a circular cylinder with diameter 2R = 3 mm and height L = 4.8 mm. We also studied another geometry with diameter 2R = 3 mm, and height L = 6 mm (results are given in Fig. S5–S7 in ESI†). In the following, unless otherwise specified, the results are for

diameter 2R = 3 mm and height L = 4.8 mm which is in the same ratio as in the micro-pillar samples. We vary two geometric parameters. The first is height of contact  $H_c$  or its nondimensional form vertical overlap as  $l_z = H_c/L$ , which measures the overlap in the z or vertical direction. When  $H_c = L$  or  $l_z = 1$ , there is no offset in the z direction while  $l_z < 0$  means that the pillars can never make contact. The second parameter,  $l_x \equiv 1 - \frac{\Delta x}{2R}$ , measures the lateral overlap of the two pillars, where  $\Delta x$  is the offset between centers of two pillars in the xdirection. Thus,  $l_x = 1$  means that there is no offset in x direction while  $l_x < 0$  means that the two pillars can never contact.

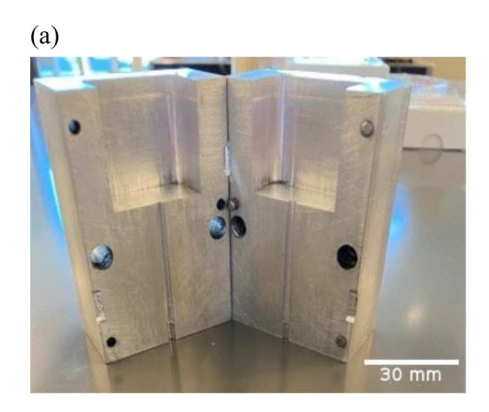
#### 2.1. Methods and materials

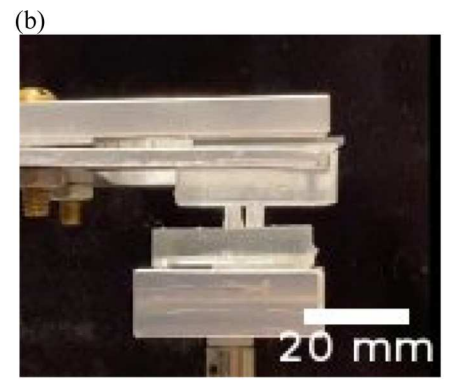
Single pillar samples are fabricated using PDMS elastomer. PDMS precursor (silicone elastomer Abase) is combined with crosslinker (curing agent, Sylgard 184 Silicone Elastomer kit, Dow Corning) in a weight ratio of 10:1. The resulting mixture is then degassed under vacuum for 30 minutes before being poured into the single pillar aluminum mold, which has been coated with a silicone-based aerosol spray. Subsequently, the mixture is cured at 80 °C for 120 minutes. Once the curing process is complete, the single pillar sample is removed from the mold and allowed to cool for a few minutes. The dimensions of cured single pillar samples are 3 mm diameter and 4.8 mm height with a backing 30 mm  $\times$  30 mm  $\times$  ~8 mm as shown in Fig. 2b.

#### 2.2. Shear and normal force during relative sliding

Shear and normal force of interaction are measured using a custom built flat-on-flat tribometer as shown in Fig. 2c. The setup consists of a stage where samples are mounted, two load cells to measure horizontal or shear force and vertical or normal force. Vertical and horizontal motors control respective direction movement of stages, and the rotation motor controls rotation of the stage. The motors are connected to a motion controller which is controlled by custom-written software in LabVIEW. A camera is used to image the behavior of pillars in a side view during sliding experiments. Shear and normal force measurements are conducted for various vertical and lateral overlaps. Lateral overlap is varied from 100% to 0%, specifically,  $l_r = 1, 0.75, 0.5, 0.25, 0$  and height of contact  $(H_c)$  is varied from 4.8 mm to 0.8 mm. A typical experiment consists of sticking the top and bottom samples to glass slides using uncured PDMS and curing at 80 °C for 30 minutes. The samples are then brought in contact under displacement control using the vertical motor. The two pillars are made to slide past each other for  $\sim 14$  mm at 0.05 mm s<sup>-1</sup>. The top sample slides with respect to the bottom sample under displacement control, and shear and normal load are recorded with respect to sliding displacement, and data are saved in a text file.

The progression of contact for the case of no lateral offset or full overlap,  $l_x = 1$  and  $l_z = 1$  is shown in Fig. 7c-h in Part I.<sup>18</sup> These figures clearly show the complicated change in geometry (large rotation in concert with stick-slip) as the two pillars make





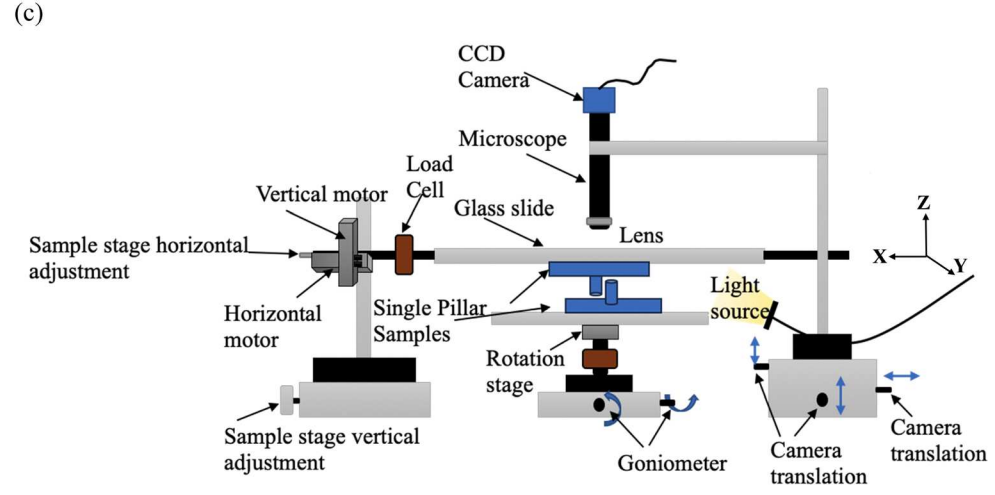


Fig. 2 (a) Aluminum mold for single pillar sample. (b) Optical micrograph of SPP samples approaching contact. (c) Schematic of custom-built flat on flat Tribometer.

and lose contact as they move past each other. For more details, please see Exp1.mp4 in ESI† Video S1.

### 3. Finite element model

All simulations were carried out using dynamic implicit (quasistatic) (DIQ) solver in ABAQUS.<sup>19</sup> The dimensions of the substrate are 15 mm  $\times$  15 mm  $\times$  9 mm. In all simulations, we fixed the bottom of one substrate, then moved the bottom of the other substrate horizontally with a constant velocity of  $\nu = 0.2 \text{ mm s}^{-1}$ while fixing the total distance between the substrates in the z direction (the result of velocity convergence tests is given in Fig. S1 in ESI†). (Because the system is nearly quasi-static, the value of the velocity is essentially irrelevant. Specifically, the role of viscoelasticity in this 10:1 PDMS is negligible.) Eight-node linear hybrid brick elements (C3D8RH) were used in all simulations. A typical mesh geometry used in our simulation is shown in Fig. 3.

Since PDMS is practically incompressible, in our simulations, we represented it by a compressible neo-Hookean solid with a bulk modulus 100 times that of the shear modulus. Contact interaction between pillars was modeled using a Coulomb friction model with a constant friction coefficient  $\mu$ . Recall that the pillars are made of PDMS, which has a shear modulus less than 1 MPa. The modulus used in our simulations is determined by comparing the horizontal and normal reaction forces for small horizontal displacements in our simulations  $(l_x = 1)$  with experimental data. This comparison gives a shear modulus of 0.65 MPa which is consistent with literature values. 20 The shear modulus is then fixed at this value for all simulations with different overlaps. This means that the friction coefficient  $\mu$  is the only remaining fitting parameter.

We also carried out mesh convergence tests using different sized meshes for pillars and substrate (see Fig. S2 in ESI†). The average size of the pillar mesh is  $s \text{ mm} \times s \text{ mm} \times s \text{ mm}$  with s = 0.5, 0.4, 0.3, 0.2, 0.1. The mesh of the substrate increases from s mm  $\times$  s mm  $\times$  1 mm near the pillar to 1 mm  $\times$  1 mm  $\times$ 1 mm near the free edges. We use the reaction force in the horizontal direction (shear force), Fs, versus the horizontal displacement u as a criterion for convergence. In ESI,† we show that for sufficiently fine meshes, specifically, when s < 0.5 mm, the  $F_{\rm s}$  versus u curves converge onto each other.

#### 4. Results

In the following, the reaction forces in the x and z direction will be called the shear and normal forces, respectively. The shear

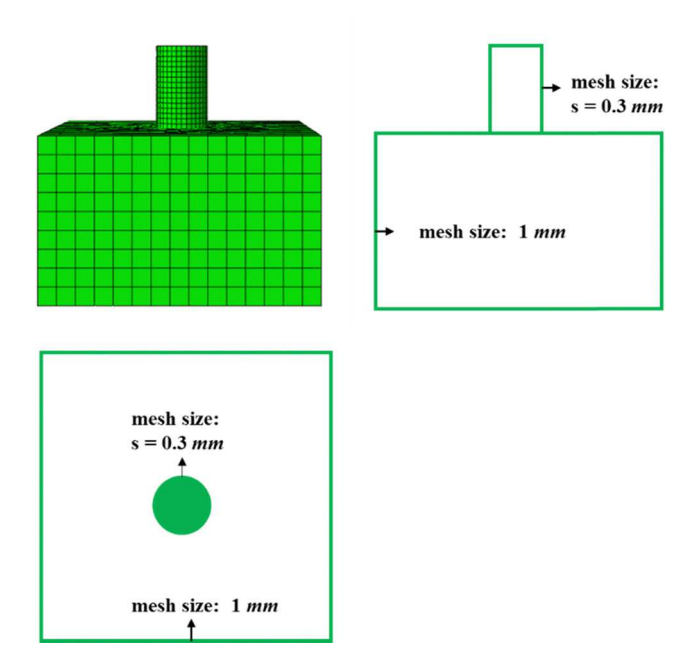


Fig. 3 Mesh geometry used for FE modeling. The mesh for the pillars is approximately uniform with size roughly equal to 0.3 mm. The substrate has a variable size mesh, with the small mesh size near the pillar, increasing to 1 mm near the edges.

and normal forces in experiments (symbols) and FE results (solid lines) for the case of  $l_x$  = 1 and five heights of contact  $H_c$ are shown in Fig. 4. To compare FE solutions with data, we fit a straight line to the initial part of experimental data to find the origin where the shear force is zero.

Fig. 4a shows that for each  $H_c$ , the shear force increases almost linearly with displacement u until  $\sim$  A. Then it increases at a slower rate until the shear force reaches a maximum at  $\sim$  B. During this time, the pillars make contact and bend in opposite directions. At peak B, contact becomes unstable, and the two pillars slip past each other and eventually (see FE1.mp4 in ESI† Video S2). Comparing Fig. 4a and b, we see that while the shear force keeps increasing before peak, the normal force reaches a maximum between A and B ( $\sim$ C), then drops and increases again after the peak C.

To understand this phenomenon, we check the magnitude of 'real' friction contact force (CS) as well as the 'real' normal force (CN) in the contact region and calculate the ratio of 'real' friction force CS to 'real' normal force CN as CS/CN. These contact forces are calculated in ABAQUS by summing the shear and normal forces over elements in the contact patch. The FE result for  $l_z$  = 2.8/4.8 or  $H_c = 2.8$  mm is shown in Fig. 5b. According to the Coulomb friction model, the ratio of contact friction force and contact normal force CS/CN should be exactly 0.4 if slip occurs. The contact surface should be locked (no slip) if this ratio is less than 0.4. The result in Fig. 5b indicates that slip occurs during small displacement up to A. Note that CS/CN is less than 0.4 between A and B, that is, in this region, the pillars stick with no global slip. More interesting is that during the initial period when slip occurs, the top pillar slips downwards with a horizontal/ vertical component in the negative y/z direction (see Fig. 5c and FEcontact.mp4 in ESI† Video S3). After the sticking period, the direction of slip is reversed, the top pillar now slips upwards with a horizontal/vertical component in the positive y/z direction.

In Fig. 6 and 7, we present results for two other lateral overlaps. The shear and normal forces versus horizontal displacement u are given in Fig. 6 for  $l_x = 0.75$  and five vertical offsets. Experimental data and FE results are represented by symbols and solid lines, respectively. As expected, lateral offset reduces the contact area which lowers the contact forces. Although the FE simulation using a friction coefficient of  $\mu$  = 0.4 did a reasonable job in fitting the experimental data, the best fit occurs at a slightly higher friction coefficient of 0.5. The simulation result for the case of  $\mu = 0.4$  is given in Fig. S3 (ESI†).

Fig. 7 plots the shear and normal forces for  $l_x = 0.5$ . Similar to the case of  $l_x = 0.75$ , we found it is necessary to increase the friction coefficient in FE simulations to obtain the best fit. For this case, we use  $\mu = 0.6$ . The results using  $\mu = 0.4$  for case with  $l_x = 0.5$  are shown in Fig. S4 (ESI†).

To summarize, our FE results based on Coulomb friction model agree well with the experimental data, especially

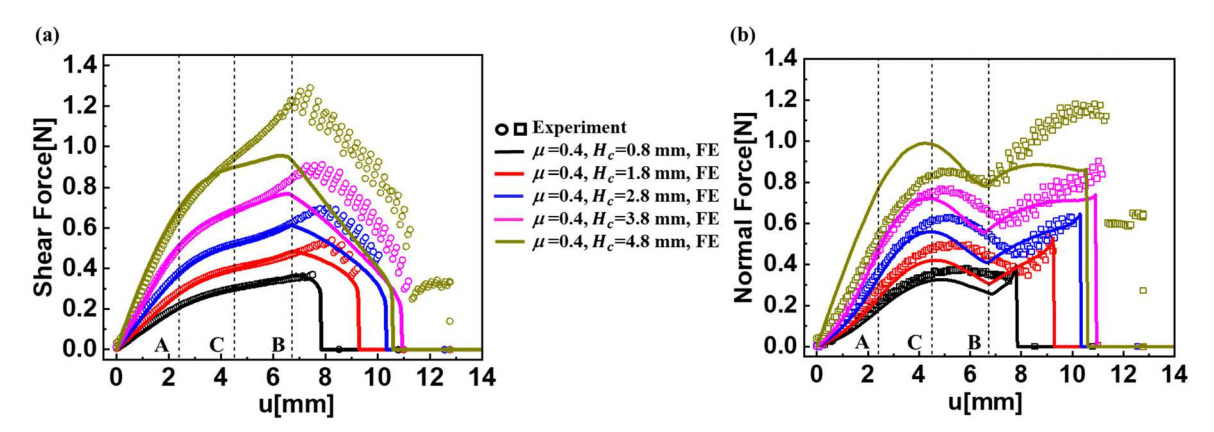


Fig. 4 FE simulation results (solid lines) ( $\mu = 0.4$ ) & experimental results (circles) for 5 heights of contact  $H_c$  with  $l_x = 1$  (no lateral offset), L = 4.8 mm and 2R = 3 mm. (a) Shear force versus horizontal displacement u, A and B correspond to u where significant slope changes occur. (b) Normal force versus u. The normal force reaches a peak at C before the pillars separate.

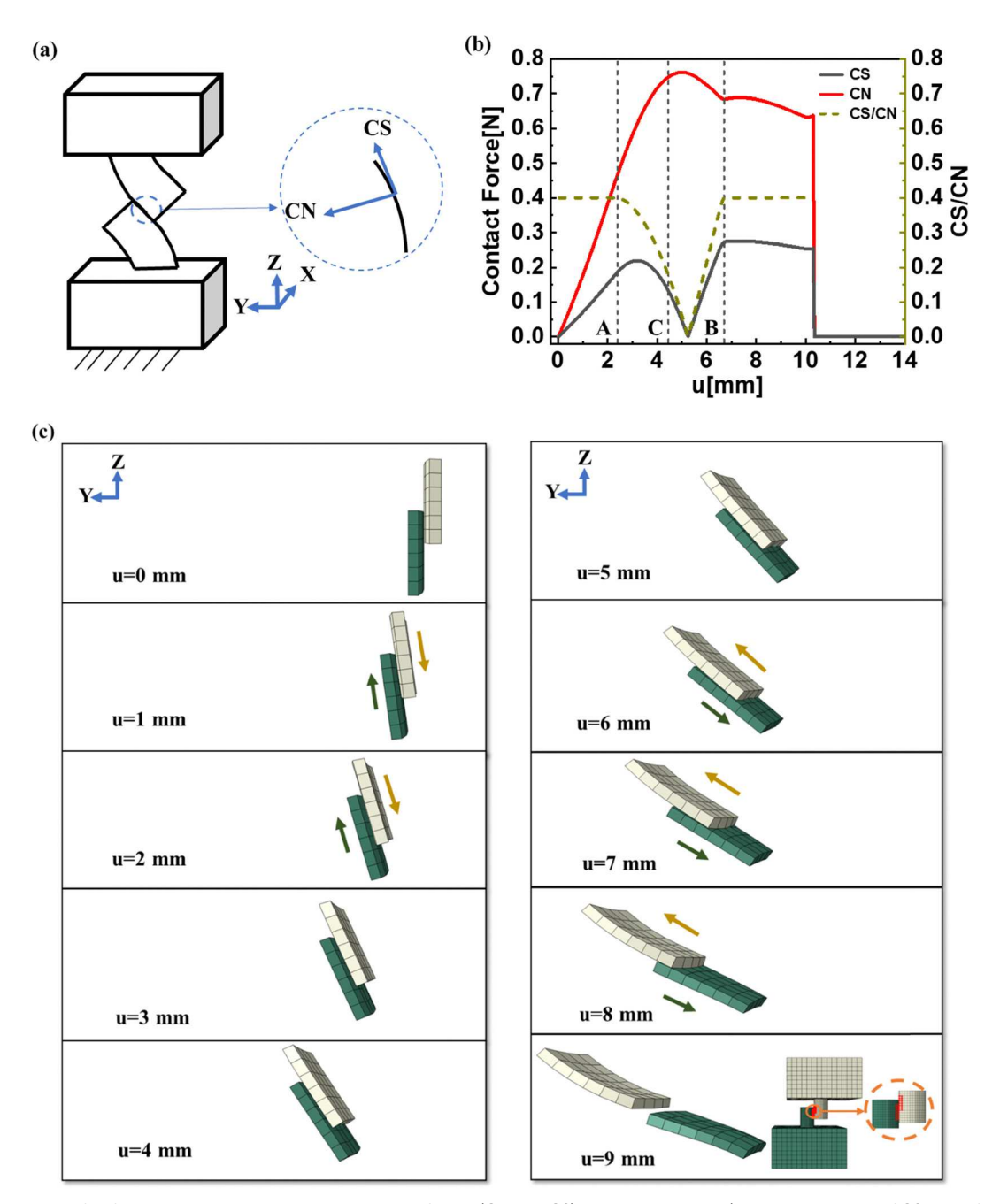


Fig. 5 (a) Schematic of deformed pillars. The inset shows contact forces (CN and CS) on the lower pillar (note the direction of CS is not fixed, it changes with the relative motion of the two pillars). (b) Contact forces vs. displacement u for  $H_c = 2.8$  mm with  $I_x = 1$  (no lateral offset). The friction coefficient in simulation is 0.4. The part of the dashed line that is horizontal corresponds to slip, i.e., CS/CN =  $\mu$ . Note pillars stick between A and B, i.e., CS/CN <  $\mu$ . (c) Snapshots of two set of elements between two pillars as sliding progresses in a FE simulation with  $H_c = 2.8$  mm with  $l_x = 1$  (or no lateral offset).

considering the large changes in geometry during sliding contact and the simplicity of the friction model. There are some discrepancies between simulation and experiments. Specifically, for any fixed  $l_x$ , the greatest deviation between experiment and simulation occurs when  $l_z = 1$  ( $H_c = L$ ). This discrepancy is understandable, since for this case, the ends of the pillars will rotate and contact with the substrate surface and this interaction is not fully accounted for in our simulations. In addition, we need to increase the friction coefficient to best fit the data as the lateral offset increases. This result is inconsistent with the fact that the samples are made of the same material. An explanation for this discrepancy will be given in the discussion.

## 5. Summary and discussion

In this work, we studied the behavior under relative sliding of individual pillar pairs with different lateral overlaps and

**Paper** Soft Matter

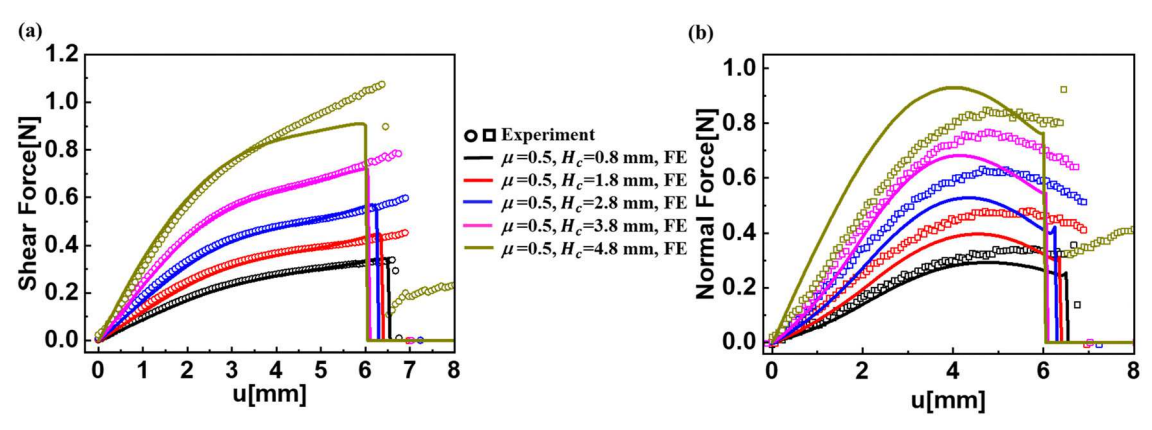


Fig. 6 FE simulation results (solid lines) ( $\mu = 0.5$ ) & experimental results (circles) for 5 different heights of contact  $H_c$  with  $I_x = 0.75$ . (a) Shear force versus horizontal displacement u. (b) Normal force versus u.

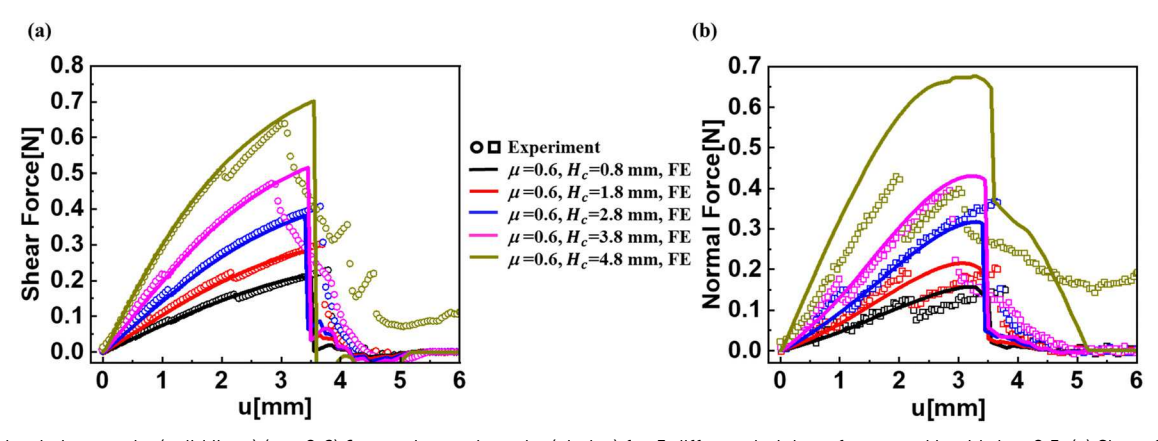


Fig. 7 FE simulation results (solid lines) ( $\mu = 0.6$ ) & experimental results (circles) for 5 different heights of contact  $H_c$  with  $l_x = 0.5$ . (a) Shear force versus horizontal displacement u. (b) Normal force versus u.

vertical overlaps experimentally and by FE simulations. We found that our 3D FE model along with a Coulomb friction model for the contacting surface captured all the complex features of experimental measurements, but with different friction coefficients. For fixed lateral offsets, the constant friction coefficients for different vertical offsets are the same. The friction force and normal force increase with larger vertical overlap,  $l_z$  (or larger  $H_c$ ) at the same displacement. For changing lateral offsets, the constant friction coefficients need to change to obtain the best fit. Specifically, the constant friction coefficient is 0.4, 0.5, 0.6 for  $l_x = 1$ ,  $l_x = 0.75$ ,  $l_x = 0.5$ , correspondingly.

The increase in friction coefficient needed to fit data suggests that the Coulomb friction model with constant friction coefficient is too simple to represent the interfacial interaction between single pillars. Even if the Coulomb model is valid, our model ignores adhesive interaction between pillars. With smaller contact area due to lateral offset, adhesive interaction will start to play an important role in comparison with friction force. Specifically, when we decrease  $l_x$ , the contact area decreases, however, this decrease is modulated by adhesion, which is not accounted for in our model. As a result, we need to use a larger friction coefficient to make up for the forces caused

by adhesive interaction. To illustrate this idea, let us consider the much simpler case of a small rigid sphere of radius R in adhesive contact with a soft incompressible elastic substrate with shear modulus, G. When the contact radius is large, adhesion can be ignored, and the contact radius a is well estimated by the Hertz theory,21

$$a = \left(\frac{3RN}{16G}\right)^{1/3},\tag{1}$$

where N is the normal compressive load acting on the sphere. For this case, the shear force S require to slide the contact can be estimated by integrating the Hertz pressure using the Coulomb friction model, which is found to be exactly  $\mu N$ (see ESI†).

On the other hand, consider the situation where the normal force N is zero, so adhesion dominates. Recall that Johnson-Kendall-Roberts theory (JKR)<sup>21</sup> showed that there is a finite contact radius  $a_0$  for the case of N = 0, *i.e.*,

$$a_0 = \left(\frac{9\pi W_{\rm ad} R^2}{8G}\right)^{1/3} \tag{2}$$

where  $W_{\rm ad}$  is the work of adhesion. Note that if we ignore adhesion, then the Coulomb model would predict S = 0 since N = 0. However, if we include adhesion, then S is not zero. Specifically, the pressure distribution inside the contact region is a combination of compression and tension such that N = 0. The region of compression occupies the circle with radius  $c < a_0$  where  $c/a_0 = \sqrt{2/3}$  (see ESI†). If we assume the region subjected to tension cannot give rise to friction, then the friction force S caused by adhesive contact can be obtained by integrating the compressive stress inside the circle of radius c using the Coulomb model, which is (see ESI†)

$$S = \frac{4\pi\mu W_{\rm ad}R}{\sqrt{3}}\tag{3}$$

Thus, adhesive contact would predict a finite shear force even if the net normal force is zero. Note for this special case there is no external normal load, so the shear force is directly proportional to the work of adhesion.

While it is possible to include adhesion in our simulation model, for example, by covering the pillar surfaces with cohesive elements, the computational difficulties are challenging. Indeed, further controlled experiments need to be performed to understand the role of adhesion in small contact situations. Further, we cannot rule out the possibility that Coulomb friction may not be the correct model for the self-contact of PDMS and that other friction models may have to be considered. For example, Chateauminois and Fretigny<sup>22</sup> have measured the local shear stress due to steady sliding of a smooth glass sphere on a smooth PDMS substrate and found that this sliding stress is approximately constant and independent of the normal force acting on the sphere. Their results indicate that Coulomb friction does not apply to smooth glass/PDMS surface. However, it is important to note that in our experiments, the contact is between PDMS surfaces. Furthermore, the surfaces of our PDMS samples are rough due to the fabrication process, which is different from the smooth surfaces used in ref. 22 As a result, the sliding friction behavior can be significantly different from that observed on smooth PDMS/glass surfaces in ref. 22. To justify our usage of Coulomb model, we conducted independent friction experiments (see ESI†). Briefly, in these additional experiments, we pressed a PDMS pillar against another PDMS pillar, with the pillars positioned at a right angle to each other, and then induced sliding motion. The results of our friction experiments strongly support the applicability of the Coulomb friction model. In addition, the observed friction coefficient aligns closely with the values utilized in our simulations. These findings provide further validation for our choice of the Coulomb model in describing the friction behavior in our study.

Finally, our simulation differs from the experiments which show that stick-slip often occurs near the shear force peak (B in Fig. 4). This behavior is not captured by our simulation since our solver is quasi-static.

In conclusion, our experiments quantify how friction and normal forces change with different lateral and vertical offsets for single pillar systems. This result provides a quantitative

method to understand how offsets of a surface architecture with pillar array control sliding friction as shown in our companion paper (refer to Part I).18 Finally, our simulation technique can be extended to study single side contact for pillar interfaces on flat substrates.

#### Data Availability

The data presented in this paper are available from the authors on reasonable request.

#### Conflicts of interest

The authors declare no conflict of interest.

### Acknowledgements

The authors acknowledge the support from the National Science Foundation, LEAP-HI: CMMI-1854572. We would also like to acknowledge useful discussions with Mike Andrews.

#### References

- 1 J. Z. Ge, A. A. Calderón, L. Chang and N. O. Pérez-Arancibia, An earthworm-inspired friction-controlled soft robot capable of bidirectional locomotion, Bioinspiration Biomimetics, 2019, 14, 036004, DOI: 10.1088/1748-3190/aae7bb.
- 2 Y. Tian, N. Pesika, H. Zeng, K. Rosenberg, B. Zhao, P. McGuiggan, K. Autumn and J. Israelachvili, Adhesion and friction in gecko toe attachment and detachment, Proc. Natl. Acad. Sci. U. S. A., 2006, 103, 19320-19325, DOI: 10.1073/pnas.0608841103.
- 3 E. Arzt, S. Gorb and R. Spolenak, From micro to nano contacts in biological attachment devices, Proc. Natl. Acad. Sci. U. S. A., 2003, 100, 10603-10606, DOI: 10.1073/pnas.1534701100.
- 4 N. J. Glassmaker, A. Jagota, C.-Y. Hui and J. Kim, Design of biomimetic fibrillar interfaces: 1. Making contact, J. R. Soc., Interface, 2004, 1, 23-33, DOI: 10.1098/rsif.2004.0004.
- 5 H. Yao and H. Gao, Mechanics of robust and releasable adhesion in biology: Bottom-up designed hierarchical structures of gecko, J. Mech. Phys. Solids, 2006, 54, 1120-1146, DOI: 10.1016/j.jmps.2006.01.002.
- 6 L. Ge, S. Sethi, L. Ci, P. M. Ajayan and A. Dhinojwala, Carbon nanotube-based synthetic gecko tapes, Proc. Natl. Acad. Sci. U. S. A. U. S. A., 2007, 104, 10792-10795, DOI: 10.1073/pnas.0703505104.
- 7 S. Gorb, M. Varenberg, A. Peressadko and J. Tuma, Biomimetic mushroom-shaped fibrillar adhesive microstructure, J. R. Soc., Interface, 2006, 4, 271-275, DOI: 10.1098/rsif.2006.0164.
- 8 B. Aksak, M. P. Murphy and M. Sitti, Adhesion of Biologically Inspired Vertical and Angled Polymer Microfiber Arrays, Langmuir, 2007, 23, 3322-3332, DOI: 10.1021/la062697t.
- 9 H. Lee, B. P. Lee and P. B. Messersmith, A reversible wet/dry adhesive inspired by mussels and geckos, Nature, 2007, 448, 338-341, DOI: 10.1038/nature05968.

- 10 L. F. Boesel, C. Greiner, E. Arzt and A. del Campo, Gecko-Inspired Surfaces: A Path to Strong and Reversible Dry Adhesives, Adv. Mater., 2010, 22, 2125–2137, DOI: 10.1002/ adma.200903200.
- 11 Q. Liu, *et al.*, Adhesion Enhancement of Micropillar Array by Combining the Adhesive Design from Gecko and Tree Frog, *Small*, 2021, **17**, 2005493, DOI: **10.1002/smll.202005493**.
- 12 B. Aksak, M. Sitti, A. Cassell, J. Li, M. Meyyappan and P. Callen, Friction of partially embedded vertically aligned carbon nanofibers inside elastomers, *Appl. Phys. Lett.*, 2007, 91, 061906, DOI: 10.1063/1.2767997.
- 13 L. Qu, L. Dai, M. Stone, Z. Xia and Z. L. Wang, Carbon Nanotube Arrays with Strong Shear Binding-On and Easy Normal Lifting-Off, *Science*, 2008, 322, 238–242, DOI: 10.1126/science.1159503.
- 14 C. Majidi, *et al.*, High Friction from a Stiff Polymer Using Microfiber Arrays, *Phys. Rev. Lett.*, 2006, **97**, 076103, DOI: **10.1103/PhysRevLett.97.076103**.
- 15 L. Shen, N. J. Glassmaker, A. Jagota and C.-Y. Hui, Strongly enhanced static friction using a film-terminated fibrillar interface, *Soft Matter*, 2008, 4, 618, DOI: 10.1039/b714737f.

- 16 M. Varenberg and S. N. Gorb, Hexagonal Surface Micropattern for Dry and Wet Friction, *Adv. Mater.*, 2009, 21, 483–486, DOI: 10.1002/adma.200802734.
- 17 S. Kim, B. Aksak and M. Sitti, Enhanced friction of elastomer microfiber adhesives with spatulate tips, *Appl. Phys. Lett.*, 2007, **91**, 221913, DOI: **10.1063/1.2820755**.
- 18 J. Kaur, X. Xiao, C. Khripin, C.-Y. Hui and A. Jagota, Soft Matter, 2024, DOI: 10.1039/D3SM01323E.
- 19 In press. Abaqus Mechanical and Civil Engineering Simulation. See <a href="https://www.3ds.com/products-services/simulia/products/abaqus/">https://www.3ds.com/products-services/simulia/products/abaqus/</a> (accessed on 16 May 2023).
- 20 N. Moyle, H. Dong, H. Wu, C. Y. Khripin, C.-Y. Hui and A. Jagota, Increased Sliding Friction of a Lubricated Soft Solid Using an Embedded Structure, *Tribol. Lett.*, 2021, 70, 2, DOI: 10.1007/s11249-021-01540-9.
- 21 K. L. Johnson and K. L. Johnson, *Contact Mechanics*, Cambridge University Press, 1987.
- 22 A. Chateauminois and C. Fretigny, Local friction at a sliding interface between an elastomer and a rigid spherical probe, *Eur. Phys. J. E: Soft Matter Biol. Phys.*, 2008, **27**, 221–227, DOI: **10.1140/epje/i2008-10376-5**.